Effects of two testing protocols on the material model parameter identification for rubber-like materials

Author(s):
Reyes, Sergio; Vassiliou, Michalis; Agathos, Konstantinos; Konstantinidis, Dimitrios

Publication date:
2022-09

Permanent link:
https://doi.org/10.3929/ethz-b-000571690

3rd EUROPEAN CONFERENCE ON
EARTHQUAKE ENGINEERING & SEISMOLOGY
BUCHAREST, ROMANIA, 2022

Effects of two testing protocols on the material model parameter identification for rubber-like materials

Sergio Reyes - Institute of Structural Engineering, Swiss Federal Institute of Technology (ETH) Zurich, Switzerland, e-mail: sergio.reyes@ibk.baug.ethz.ch

Michalis Vassiliou – Institute of Structural Engineering, Swiss Federal Institute of Technology (ETH) Zurich, Switzerland, e-mail: vassiliou@ibk.baug.ethz.ch

Konstantinos Agathos – College of Engineering, Mathematics, and Physical Sciences, University of Exeter, UK, e-mail: k.agathos@exeter.ac.uk

Dimitrios Konstantinidis – Department of Civil and Environmental Engineering, University of California, Berkeley, USA, e-mail: konstantinidis@berkeley.edu

Abstract: This paper analyzes the polyurethane material that can be used for the construction of seismic isolation devices based on rolling of elastomeric spheres. Such isolators could be used in low-income countries. Uniaxial tensile tests were performed on dumbbell-shaped polyurethane 95 ShA specimens under two different loading protocols. Protocol 1 consisted of applying a cyclic saw-tooth loading centered on a pre-imposed initial deformation, while Protocol 2 consisted of consecutive loadings followed by relaxation at three different deformation levels. Then, a material model comprising three-chains in parallel was calibrated against the tests. The model combined the Yeoh hyperelastic and Bergstrom-Boyce models. The results of the parameter calibration showed that different testing protocols could lead to different model parameter values. In terms of fitting errors, it is observed that fitting to Protocol 1 generates a good prediction on Protocol 2 with an error of 0.26%; however, when fitting to Protocol 2, the behavior observed on Protocol 1 could not be accurately predicted, resulting in an error of 9.10%. Moreover, when comparing fitting to match only Protocol 1 with considering both protocols simultaneously, the total error is only reduced from 0.32% to 0.20%, suggesting that Protocol 2 adds redundant information already contained in Protocol 1. Additional tests with different deformation rates and ranges need to be conducted to define an optimal protocol for material calibration.

Keywords: Bergstrom-Boyce, Yeoh hyperelastic, hyperelasticity, rubber modeling, parameter calibration, parallel rheological framework, testing protocol.

1. Introduction

Seismic isolation has matured during the last decades. However, its application in low-income countries is very limited for several reasons, including the cost of the isolators themselves. Several isolation devices that have the potential to be manufactured at a low cost have been proposed, including the Fiber Reinforced Elastomeric Isolators (FREIs) (Kelly, 1999; Kelly & Konstantinidis, 2011; Naeim & Kelly, 1999) and the Spherical Deformable Rolling Seismic Isolator (SDRSI) (Cilsalar & Constantinou, 2019; Katsamakas et al., 2021, 2022) (Figure 1, top). The latter uses an elastomeric sphere rolling on a concave concrete surface. Typically, FREIs would use a soft rubber compound, while SDRSIs would require much harder compounds (harder than 95A). Moreover, typically FREIs would mainly involve shear deformation, while the strain state of a rolling elastomeric sphere is more complicated and would also involve compression

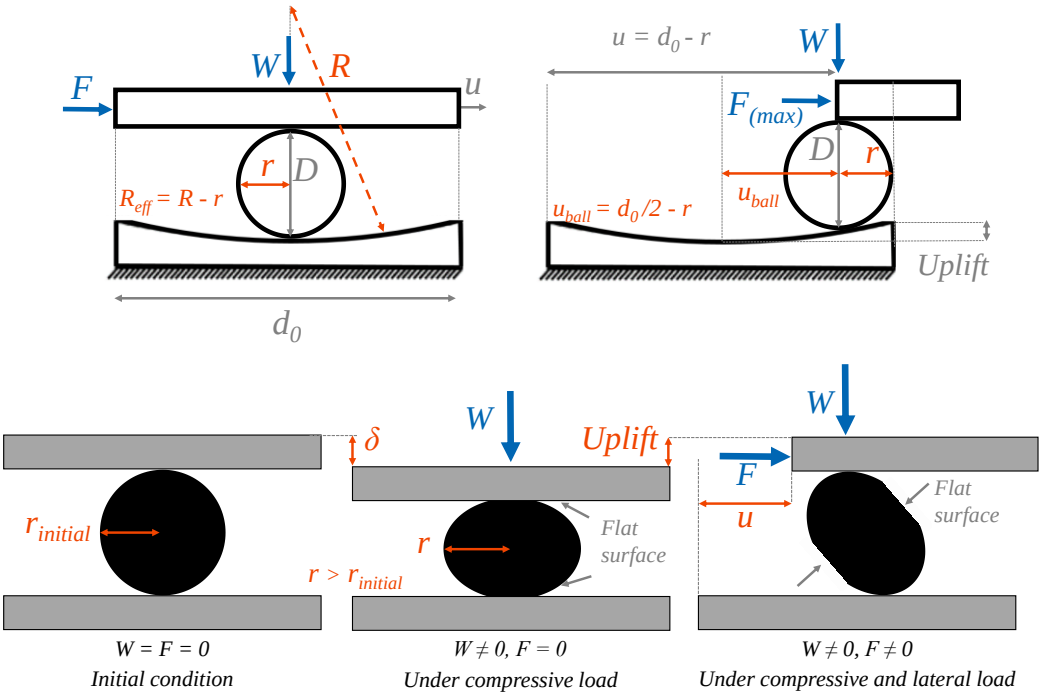

Figure 1. Top: The Spherical Deformable Rolling Seismic Isolator (rigid body approximation) Bottom: Influence of the flexibility of the rubber (from Katsamakas et al., 2022)

and tension, a strain state that also appears in other rubber isolation devices (Reyes et al., 2020, 2022; Reyes & Almazán, 2020).

First results have shown that the behavior of SDRSIs is more complicated than that of a rigid sphere rolling on a spherical surface. The sphere deforms under creep and develops flat spots against the top and bottom support surfaces. When it rolls, its oblong shape results in non-smooth rolling motion (Figure 1, bottom). The behavior of such a system depends on the elastic, creep, and cyclic behavior characteristics of the elastomeric material. Modelling such rolling behavior requires a material constitutive law that takes into account rate dependence (as there is both creep and rate dependence of the rolling behavior), as well as damage (as the spheres creep to flattened spheres under compression but do not recover their original shape when the load is removed).

Calibrating material models for elastomeric materials under different strain conditions and different deformation modes (e.g., tension, shear, and biaxial extension) would be ideal, but performing several physical experiments is highly expensive and time-consuming. However, it has been shown that uniaxial tensile tests (ASTM, 2018) can provide reliable information on the behavior under other deformation modes, as well (Bergstrom, 2015; Forouzesh & Azadi, 2011; Beckmann et al., 2018).

This paper proposes a model to describe the behavior of polyurethane of Shore hardness 95A. It then proceeds with evaluating the effect of considering two different uniaxial testing protocols on the calibration of the material parameters. This is done on water-cut standardized dumbbell tensile specimens obtained directly from a polyurethane ball used for tests on SDRSIs.

2. Description of the experimental campaign

2.1. Dumbbell specimen

The polyurethane ball considered in this study had a nominal Shore A hardness of 95 ± 5. Purchasing standardized tensile dumbbell specimens together with the balls coming from the same material batch was not possible due to manufacturer production line restrictions. Thus, the specimens for the material parameter calibration were obtained directly from a 100 mm diameter ball with a water-jet cutting machine.

The ball was cut into two-millimeter slices, from where the tensile specimens were later obtained. Figure 2 presents the water-jet cutting process and the final dumbbell tensile specimens. Type 2, Type 3, and Type 4 specimens (according to ISO37 standard) were obtained; however, only results associated with Type 2 specimens are reported herein.

The water-cutting machine parameters were set to 4500 Bar of pressure and 250 g/m of sand on a 0.5 mm cutting system. Cutting the slices out from the ball was performed at a considerably lower speed (by a factor of 25, approximately) than cutting the specimens out from the slices.

2.2. Applied displacement protocols

Two displacement protocols were applied on the same preconditioned Type 2 tensile specimen. These protocols were named Protocol 1 and Protocol 2, respectively. The first protocol consisted of cyclic saw-tooth loading centered on a pre-imposed initial deformation. The second protocol consisted of consecutive loadings followed by relaxation at three different deformation levels. In both cases, loading, unloading, and reloading paths were performed at engineering strain rates of 0.093 s^{-1}. The strain of the specimen was measured with a standard extensometer with its gauge length set at 20 mm and placed at the narrow part of the specimen. Figure 3 presents the experimental setup, the applied deformation protocols, and the obtained stretch-stress relationships.

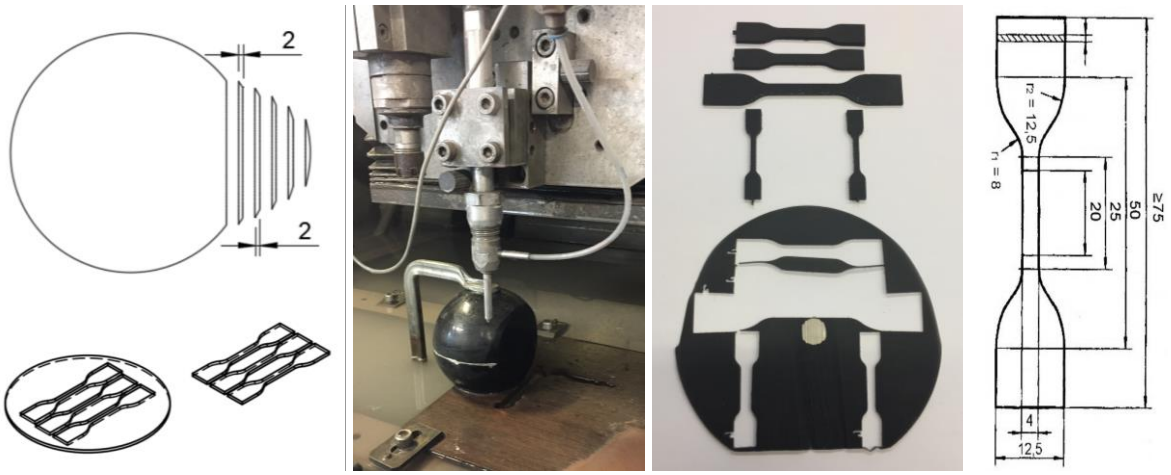

Figure 2 – From left to right: i) Cutting drawings, ii) water-jet cutting process, iii) final dumbbell specimens, iv) Type 2 ISO37 specimen. All dimensions in mm.

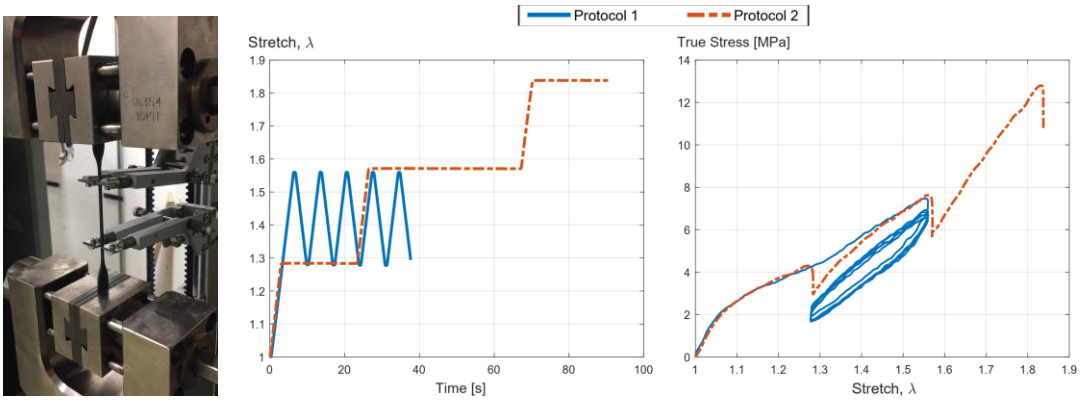

Figure 3 – Experimental setup and testing protocols

3. Constitutive modeling and equations

This section briefly presents the modeling approach and the main equations of the considered constitutive model. The constitutive model equations presented herein were chosen to be consistent with the implementation in the MSC Marc software (Marc, 2019), which may slightly differ from modern textbooks or recent papers.

The Parallel Rheological Framework (PRF) approach was used for the constitutive material modeling. This approach decouples the behavior of the material to different parallel chains with a given individual constitutive behavior. The PRF is already implemented in some FE commercial software, such as MSC MARC (MSC Software Corporation, 2019), and is helpful for modeling rubberlike materials (Marc, 2019). When modeling rubber, the standard approach is to separate the behavior of the material into a primary nonlinear hyperelastic chain (which provides the time-infinite equilibrium response) and several secondary viscoelastic chains (which provide the hysteretic and time-dependent behavior).

In this work, one primary and two secondary chains are considered, as shown in Figure 4. For the primary chain (i.e., Chain A), the Yeoh hyperelastic model is considered (Yeoh, 1993). For the secondary chains (i.e., Chains B and C), the Bergstrom-Boyce (BB) model is used, which is composed of an Eight-Chain (EC) hyperelastic model element in series with a nonlinear viscous flow element (Bergström & Boyce, 2001). For all cases, the isotropic and incompressible material formulation is considered. Figure 4 presents the rheological representation of the complete model with their respective material parameters.

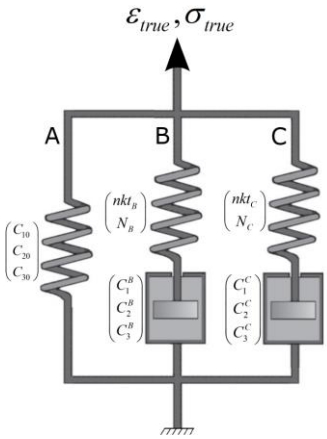

Figure 4 – Rheological representation of the constitutive material with the involved material parameters on each chain. Figure adapted from (Bergstrom, 2015).

It has been shown that the Yeoh and EC hyperelastic models have good predicting capabilities on various deformation states simultaneously while having fewer material parameters (Bergstrom, 2015). Moreover, both models depend only on the first invariant of the stretch tensor I_1, which is a better choice when only uniaxial data is available (given the strong dependence of I_2 on other deformation states, such as biaxial loading). Therefore, these models are a suitable choice for this study.

3.1. Yeoh hyperelastic model

The Yeoh hyperelastic model (Yeoh, 1993) corresponds to a phenomenological third-order polynomial that depends only on the first deformation invariant I_1, neglecting the contribution of the second invariant I_2. The strain energy function of the incompressible Yeoh model is:

$$W_{Yeoh} = C_{10}\left(I_1 - 3\right) + C_{20}\left(I_1 - 3\right)^2 + C_{30}\left(I_1 - 3\right)^3 \tag{1}$$

where C_{10}, C_{20}, and C_{30} are the model parameters, and I_1 is the first invariant of the right Cauchy-Green deformation tensor. Given the higher order I_1 terms, this model can represent S-shaped stress-stretch relationships more accurately than lower-order models. Moreover, neglecting the dependence on I_2 makes it easier to be Drucker stable (Yeoh, 1993).

3.2. Eight-Chain hyperelastic model

The EC hyperelastic model (Arruda & Boyce, 1993) corresponds to a physics-based model that assumes that the chain molecules of the material are, on average, located along the diagonals of a unit cubic cell located in the principal stretch space. The stress-strain energy function of the EC model involves the Langevin function; however, it is generally expressed as a series expansion, yielding the following expression (Marc, 2019):

$$W_{EC} = nkt\left[\frac{1}{2}\left(I_1 - 3\right) + \frac{1}{20N}\left(I_1^2 - 9\right) + \frac{12}{1050N^2}\left(I_1^3 - 27\right) + \frac{19}{7000N^3}\left(I_1^4 - 81\right) + \frac{519}{673750N^4}\left(I_1^5 - 243\right)\right] \tag{2}$$

where *nkt* and *N* are the model parameters, representing the initial modulus and limiting chain extensibility, respectively. Here, I_1 also corresponds to the first invariant of the right Cauchy-Green deformation tensor.

3.3. Nonlinear viscoelastic element on Bergstrom-Boyce model

The BB model is a constitutive model for representing the nonlinear time-dependent large-strain behaviour of elastomeric materials (Bergström, 1999; Bergstrom, 2015; Bergström & Boyce, 1998, 2000, 2001; Bergström & Boyce, 1999). According to the MSC Marc implementation, the flow rate rule of the nonlinear viscous element is given by (Marc, 2019):

$$\dot{\gamma} = C_1\left[\lambda_{chain} - 1 + \xi\right]^{C_2}\left(\tau\right)^{C_3} \tag{3}$$

where C_1, C_2, and C_3 are the model parameters, λ_{chain} is the viscous element stretch, ξ is a small positive constant (e.g., 5×10^{-3}) for stability in undeformed configurations (i.e., $\lambda_{chain} \approx 1$), and τ is the effective stress driving the viscous flow. This model considers the multiplicative decomposition of the deformation gradient (i.e., $\lambda_i = \lambda_i^e \lambda_i^p$), where the elastic part is associated with the EC model and the plastic part with the non-linear viscous element.

4. Material parameters calibration results

The considered model has a total of 13 parameters: C_{10}, C_{20}, and C_{30} for the Yeoh model in chain A; nkt_B, N_B, C_1^B, C_2^B, and C_3^B for the BB model in chain B; and nkt_C, N_C, C_1^C, C_2^C, and C_3^C for the BB model in chain C. However, parameters C_2^B and C_2^C can be set to -1 since they are constrained to be close to that value due to reptational dynamics (Bergström & Boyce, 2001; Schäfer et al., 1999).

The remaining 11 parameters were obtained under an optimization scheme using the Covariance Matrix Adaptation Evolution Strategy (CMA-ES) (Hansen & Kern, 2004). The objective function to be minimized was set as:

$$f(\sigma_i^{\exp}, \sigma_i^{pred}) = \frac{\sum_{i=1}^{n} \left(\sigma_i^{\exp} - \sigma_i^{pred} \right)^2}{\sum_{i=1}^{n} (\sigma_i^{\exp})^2} \tag{4}$$

where $\sigma_i^{\exp}$ and σ_i^{pred} are the measured and predicted stress values during the tests, respectively. The predicted stresses were obtained applying both displacement protocols to the proposed numerical model for a given case of optimal parameters. Three cases were considered for the optimization: (i) fitting the parameters to match Protocol 1 (Case A), (ii) fitting them to match Protocol 2 (Case B), and (iii) fitting to match both Protocols 1 and 2 simultaneously (Case C). Table 1 presents the optimization results, including the objective fitting protocol, search domain, the optimal parameter values, and the fitting error per protocol as a percentage (i.e., $f(\sigma_i^{\exp}, \sigma_i^{pred}) \times 100$). Parameters not included in the optimization are **bolded**.

It can be observed that for most of the parameters, the optimal values for Cases A and C are similar. Moreover, the overall error does not change much between Cases A and C (from 0.32%, it drops to 0.20%). On the contrary, when one calibrates based only on Protocol 2 (i.e., Case B), a) the model parameters are very different, and b) the total error is much larger (9.12%). Therefore, training on Protocol 1 to predict the response of Protocol

Table 1. Summary of the obtained material parameters.

		Search domain	Objective fitting protocol		
			Case A	Case B	Case C
Yeoh (Chain A)	C_{10}	[1, 2.5]	1.88	1.00	1.81
	C_{20}	[-1, 1]	-5.13×10^{-1}	1.10	-4.61×10^{-1}
	C_{30}	[0.01, 1]	2.30×10^{-1}	5.20×10^{-2}	2.16×10^{-1}
Bergstrom-Boyce (Chain B)	nkt	[0.1, 20]	2.73	1.45	2.15
	N	[1, 5]	5.00	1.00	2.10
	C_1	[0, 5]	1.25×10^{-3}	2.48×10^{-4}	8.06×10^{-3}
	C_2	**-**	**-1.00**	**-1.00**	**-1.00**
	C_3	[1, 10]	3.50	4.70	3.60
	ξ	-	**5.0×10^{-3}**	**5.0×10^{-3}**	**5.0×10^{-3}**
Bergstrom-Boyce (Chain C)	nkt	[0.1, 20]	11.8	3.59	10.3
	N	[1, 5]	3.60	4.10	3.80
	C_1	[0, 5]	5.00	1.0×10^{-2}	5.2×10^{-2}
	C_2	**-**	**-1.00**	**-1.00**	**-1.00**
	C_3	[1, 10]	7.40	5.70	2.50
	ξ	-	**5.0×10^{-3}**	**5.0×10^{-3}**	**5.0×10^{-3}**
Fitting errors $f(\sigma_i^{\exp}, \sigma_i^{pred})$ x 100	Protocol 1		0.06	9.10	0.06
	Protocol 2		0.26	0.02	0.14
	Total sum		0.32	9.12	0.20

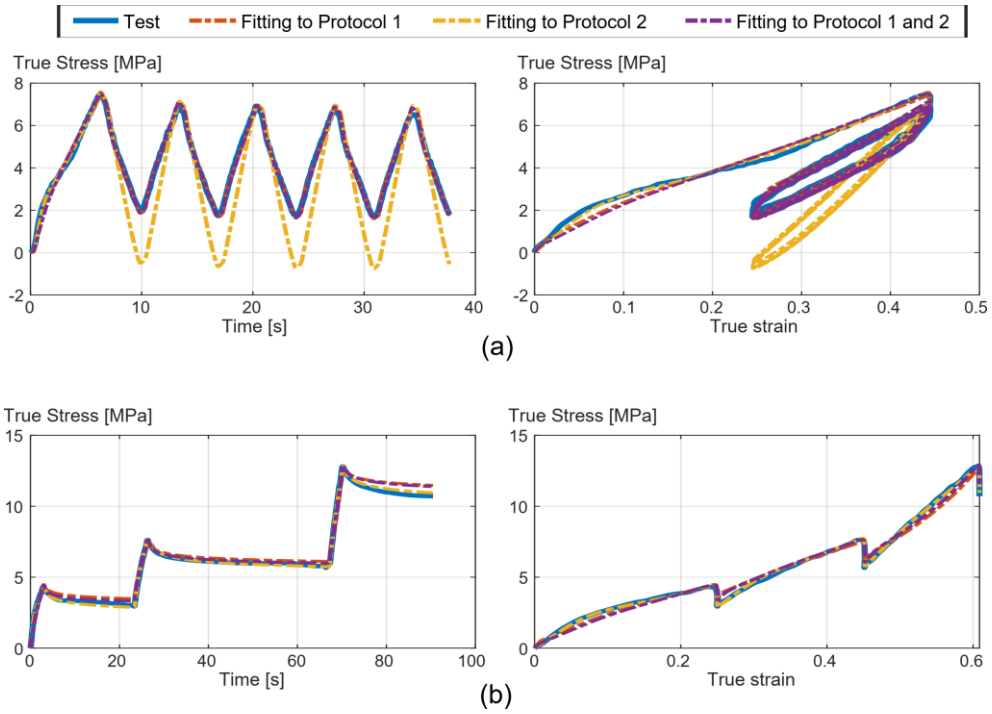

Figure 5 – Performance of the three sets of obtained parameters when the two testing protocols are applied to the proposed numerical model: (a) Protocol 1 and (b) Protocol 2.

2 is feasible, while the opposite is not. Moreover, training on both Protocols 1 and 2 simultaneously, does not seem to offer a significant advantage compared to training solely on Protocol 1. Therefore, there does not seem to be a reason to experimentally test under Protocol 2. Figure 5 presents the performance of the three sets of obtained parameters. It can be observed that, in fact, Cases A and C yielded better and similar results compared with Case B. In addition, no substantial improvement is observed in the fitting when protocol 2 is included.

Other interesting results are the *nkt* values obtained on Chains B and C. A high *nkt* value is generally associated with a stiff instantaneous (short-term) response on the chain, while a small *nkt* value with a flexible long-term behavior. In both Case A and C, the optimization procedure assigned a small and a large value in each chain, thus decoupling its long- and short-term behavior. In fact, in these cases, Chain B (small nkt value) provides the relaxation behavior, while Chain C (larger nkt value) provides the hysteretic loops.

5. Conclusions and further work

This study included uniaxial tests on a dumbbell-shaped Polyurethane specimen of 95A hardness under two different loading protocols. It proposed a three-chain parallel rheological constitutive model to compute the rate-dependent hysteretic cyclic response and evaluated the usefulness of each loading protocol. Protocol 1 consisted of applying a cyclic saw-tooth loading centered on a pre-imposed initial deformation, and Protocol 2 of consecutive loadings followed by relaxation at three different deformation levels.

The main conclusions of this work can be summarized as follows:

- The testing protocol has a strong influence on the obtained parameters since it affects the types of phenomena captured (e.g., Creep, relaxation, hysteresis, etc.)
- Performing only monotonically increasing deformation protocols (even with intermediate relaxations) does not suffice for a proper material calibration, since

information related to unloading or cyclic deformation is missing and is not captured by the model.

- Applying cyclic protocols at a fixed range of deformation during extended periods of time may provide information about the relaxation behavior as well, since relaxation behavior is observed when cycling at a pre-imposed deformation during extended periods (few seconds).
- Considering two secondary chains in the Parallel Rheological Framework gave the model an adequate response. Moreover, the obtained parameters were associated with different behaviors: (i) one chain representing the energy dissipated on cyclic deformations, and (ii) the other chain representing the relaxation behavior. The optimal number of parallel chains is still unclear and needs to be further studied.
- More tests and analyses need to be performed to define an optimal set of protocols for material characterization.
- The deterioration in time of the polyurethane mechanical properties need to be further investigated since other elastomeric devices have evidenced changes on its long-term mechanical behavior and property modification factors have been proposed (Mazza, 2019; McVitty & Constantinou, 2015).

Acknowledgments

This research has been supported by the Sawiris Foundation for Social Development and ETH for Development. The authors are grateful for the support.

References

American Society for Testing and Materials. ASTM. (2018). Designation: D 412 – 06a Standard test method for tensile properties of Vulcanized Rubber and Thermoplastic Elastomers—. *ASTM D 412-06a*, *598*, 143–152.

Arruda, E. M., & Boyce, M. C. (1993). A three-dimensional constitutive model for the large stretch behavior of rubber elastic materials. *Journal of the Mechanics and Physics of Solids*, *41*(2), 389–412. https://doi.org/10.1016/0022-5096(93)90013-6

Beckmann, A., Heider, Y., Stoffel, M., & Markert, B. (2018). Assessment of the viscoelastic mechanical properties of polycarbonate urethane for medical devices. *Journal of the Mechanical Behavior of Biomedical Materials*, *82*(December 2017), 1–8. https://doi.org/10.1016/j.jmbbm.2018.02.015

Bergström, J. (1999). Large strain time-dependent behavior of elastomeric materials. In *PhD Thesis* (p. 260). Massachusetts Institute of Technology. https://dspace.mit.edu/handle/1721.1/9794

Bergstrom, J. S. (2015). *Mechanics of solid polymers: theory and computational modeling* (2015th ed.). William Andrew, ElSevier.

Bergström, J. S., & Boyce, M. C. (1998). Constitutive modeling of the large strain time-dependent behavior of elastomers. *Journal of the Mechanics and Physics of Solids*, *46*(5), 931–954. https://doi.org/10.1016/S0022-5096(97)00075-6

Bergström, J. S., & Boyce, M. C. (2000). Large strain time-dependent behavior of filled elastomers. *Mechanics of Materials*, *32*(11), 627–644. https://doi.org/10.1016/S0167-6636(00)00028-4

Bergström, J. S., & Boyce, M. C. (2001). Constitutive modeling of the time-dependent and cyclic loading of elastomers and application to soft biological tissues. *Mechanics of Materials*, *33*(9), 523–530. https://doi.org/10.1016/S0167-6636(01)00070-9

Bergström, Jörgen S., & Boyce, M. C. (1999). Mechanical behavior of particle filled elastomers. *Rubber Chemistry and Technology*, *72*(4), 633–656. https://doi.org/10.5254/1.3538823

Cilsalar, H., & Constantinou, M. C. (2019). Behavior of a spherical deformable rolling seismic isolator for lightweight residential construction. *Bulletin of Earthquake Engineering*, *17*(7), 4321–4345. https://doi.org/10.1007/s10518-019-00626-z

Hansen, N., & Kern, S. (2004). Evaluating the CMA evolution strategy on multimodal test functions. *Lecture Notes in Computer Science (Including Subseries Lecture Notes in Artificial Intelligence and Lecture*

Notes in Bioinformatics), *3242*, 282–291. https://doi.org/10.1007/978-3-540-30217-9_29

Katsamakas, A. A., Belser, G., Vassiliou, M. F., & Blondet, M. (2022). Experimental investigation of a spherical rubber isolator for use in low income countries. *Engineering Structures*, *250*, 113522. https://doi.org/10.1016/j.engstruct.2021.113522

Katsamakas, A. A., Chollet, M., Eyyi, S., & Vassiliou, M. F. (2021). Feasibility Study on Re-Using Tennis Balls as Seismic Isolation Bearings. *Frontiers in Built Environment*, *7*, 129. https://doi.org/10.3389/fbuil.2021.768303

Kelly, J. M. (1999). Analysis of Fiber-Reinforced Elastomeric Isolators. *Journal of Seismology and Earthquake Engineering*, *2*(1), 19–34.

Kelly, J. M., & Konstantinidis, D. A. (2011). *Mechanics of Rubber Bearings for Seismic and Vibration Isolation*. John Wiley & Sons, Ltd. https://doi.org/10.1002/9781119971870

Marc, M. (2019). Volume A : Theory and User Information. *MSC. Software Corporation, Palo Alto, USA*, 867.

Mazza, F. (2019). Effects of the long-term behaviour of isolation devices on the seismic response of base-isolated buildings. *Structural Control and Health Monitoring*, *26*(4), e2331. https://doi.org/10.1002/stc.2331

McVitty, W., & Constantinou, W. (2015). Property modification factors for seismic isolators: Design guidance for buildings. *MCEER Report*, 242. http://mceer.buffalo.edu

MSC Software Corporation. (2019). *MSC Marc*.

Naeim, F., & Kelly, J. M. (1999). *Design of seismic isolated structures : from theory to practice*. John Wiley & Sons, Ltd.

Reyes, S., Almazán, J. L., Colombo, J. I., Tapia, N., & de la Llera, J. C. (2020). Shaking Table Tests on Full-Scale Legged Liquid Storage Tanks Protected With a Vertical-Rocking Isolation System. *17 World Conference on Earthquake Engineering, Sendai, Japan*, C002408. https://www.researchgate.net/publication/345507107_Shaking_table_tests_on_full-scale_legged_liquid_storage_tanks_protected_with_a_vertical-rocking_isolation_system

Reyes, S. I., & Almazán, J. L. (2020). A novel device for a vertical rocking isolation system with uplift allowed for industrial equipment and structures. *Engineering Structures*, *214*. https://doi.org/10.1016/j.engstruct.2020.110595

Reyes, S. I., Almazán, J. L., Vassiliou, M. F., Tapia, N. F., Colombo, J. I., & de la Llera, J. C. (2022). Full-scale shaking table test and numerical modeling of a 3000-liter legged storage tank isolated with a vertical rocking isolation system. *Earthquake Engineering and Structural Dynamics*. https://doi.org/10.1002/eqe.3628

Schäfer, L., Baumgärtner, A., & Ebert, U. (1999). Reptational dynamics of a polymer chain is stable against kinematic disorder. *European Physical Journal B*, *10*(1), 105–117. https://doi.org/10.1007/s100510050834

Yeoh, O. H. (1993). Some forms of the strain energy function for rubber. *Rubber Chemistry and Technology*, *66*(5), 754–771. https://doi.org/10.5254/1.3538343